PROCEEDINGS OF SCIENCE

Strong coupling lattice study of $1/g^2$ evolution in phase diagram and baryon mass

Kohtaroh Miura* **and Akira Ohnishi**
Yukawa Institute for Theoretical Physics, Kyoto University, Kyoto 606-8502, Japan
E-mail: miura@yukawa.kyoto-u.ac.jp

Noboru Kawamoto

Hokkaido University, Hokkaido, Sapporo 060-0810, Japan

We investigate the phase diagram and the baryon mass ($M_{\rm B}$) in the color SU($N_c = 3$) strong coupling lattice QCD with one species of staggered fermions at finite quark chemical potential (μ) and/or finite temperature (T). In particular, their evolution with the finite coupling ($1/g^2$) is studied in the next to leading order of the strong coupling expansion. We formulate the treatment of the temporal plaquette effects by introducing some new kinds of mean fields, which lead to the suppression of μ and the constituent quark mass (m_q). These energy scale modifications cause the following phase diagram evolution: (1) The ratio of the critical value (μ_c/T_c) becomes closer to the empirical value. (2) As the coupling decreases, the second order transition at zero chemical potential evolves to the first order, and the critical temperature T_c is found to be consistent with lattice Monte-Carlo simulations. The same suppression mechanism of μ also modifies the analytic relation between the baryon mass $M_{\rm B}$ and the critical baryon chemical potential ($N_c\mu_c$). We show that the ratio $N_c\mu_c/M_{\rm B}$ grows as the coupling decreases, and this trend may be helpful to form the nuclear matter in the current frame work.

The XXVI International Symposium on Lattice Field Theory
July 14-19 2008
Williamsburg, Virginia, USA

*Speaker.

1. Introduction

Exploring the phase diagram of Quantum Chromodynamics (QCD) has recently attracted much attention due to the developments in the heavy-ion collision experiments. The Relativistic Heavy-Ion Collider (RHIC) has shown intriguing experimental findings: the formation of strongly interacting Quark Gluon Plasma (sQGP) [1]. Further developments are also expected in the ALICE experiment in the Large Hadron Collider (LHC). Compressed baryonic matter can be created in heavy-ion collision experiments at lower energies (FAIR and so on), and cold and dense baryonic matter is realized in the core of neutron stars. In the high density region, various interesting phases have been proposed so far: the color superconductor [2], and the quarkyonic matter [3] *etc.* Unfortunately, the lattice MC simulations is difficult to access to this region because of the notorious negative sign problem of the Dirac determinant. Many ideas have been proposed, and the relatively small density region becomes accessible by using MC simulations [4]. However the alternative methods may be needed to investigate the whole structure of the phase diagram including the low temperature and high density region.

Here the effective model would be a possible approach, and in fact, there are many successful effective models in the study of the QCD phase diagram. In this proceedings, we adopt a more direct method which is based on the strong coupling expansion (expansion in the inverse of the squared bare coupling, $1/g^2$) in the lattice QCD. In 1980's, the sophisticated methods were developed in the staggered fermion formalism [5 – 8], in order to investigate the chiral phase transition. There the sign problem could be avoided in the mean field approximation. This *Strong Coupling Lattice QCD* (SC-LQCD) is based on the same formulation as the lattice MC simulations, therefore the results of the former should be reproduced by the latter in the strong coupling region. Such a kind of comparison plays an important role to obtain a firm confirmation of the formulation and numerical results. We shall explicitly perform that in the phase diagram study.

Recently the transition order and the location of the critical end point have become fascinating topics. In this point of view, some remarkable developments in SC-LQCD can be found in the recent few years: In the strong coupling limit (SCL, $1/g^2 \to 0$), the phase diagrams have been precisely investigated in the SU(2) [9] and SU(3) [10, 11] cases. It is interesting to consider the finite coupling cases, and to investigate the phase diagram evolution with $1/g^2$ effects. Then the key quantity may be the ratio $R = \mu^{\rm cri}_{T=0}/T^{\rm cri}_{\mu=0}$ in the following reason. In our previous work [11], we pointed out that R might be much smaller than the empirical value. The lattice MC simulations suggest that the critical end point locates in the region $\mu/T > 1$. This indicates $R \gg 1$, while the strong coupling limit shows $R \sim 0.3 - 0.45$. Since SC-LQCD should be consistent with the lattice MC at strong coupling, the finite coupling effect should improve the critical ratio R.

Another interesting problem in the SC-LQCD is the *Baryon Mass Puzzle (BMP)*: Naïvely, the chiral phase transition is expected to occur when a baryon chemical potential $N_c\mu$ approaches to the baryon mass $M_{\rm B}$, *i.e.* $N_c\mu_c \simeq M_{\rm B}$ [7]. From a more practical point of view, the relation $N_c\mu_c > M_{\rm B}$ may be preferable to form nuclei. Contrary to these expectations, previous studies based on the strong coupling limit of lattice QCD indicate the relation $N_c\mu_c < M_{\rm B}$. This BMP problem has been known since 1980's, and confirmed in the lattice MC study [12, 13]. The MC result for $M_{\rm B}$ at strong coupling [12] is quite larger than $N_c\mu_c$ semi-analytically obtained in the strong coupling limit. For this problem, the previous work [14] indicated that the finite coupling makes $N_c\mu_c$ larger

and closer to the $M_{\rm B}$ [15]. And the analytic relation between $N_c\mu_c$ and $M_{\rm B}$ is recently indicated in the strong coupling limit by B. Bringoltz [16].

In this proceedings, we investigate the phase diagram and the baryon mass $M_{\rm B}$ in the strong coupling lattice QCD with one species of staggered fermions at finite quark chemical potential (μ) and/or finite temperature (T) . This is along the line of our previous investigations [11, 17 – 21]. In particular, the $1/g^2$ evolution in the next to leading order of the strong coupling expansion is studied. We formulate the treatment of the temporal plaquette effects by introducing some new kinds of mean fields, which lead to the suppression of μ and the constituent quark mass (m_q). Then we investigate evolution of the phase diagram with finite coupling effects in a finite T treatment. The same suppression mechanism of μ also modifies the analytic relation between the baryon mass $M_{\rm B}$ and the critical baryon chemical potential ($N_c\mu_c$). This analysis provides the extension with the finite coupling to the later part of the work [16]. Although the BMP with $1/g^2$ effects has been investigated in Ref. [14], the present work could give some additional knowledge: Firstly we provide the analytic relation between $N_c\mu_c$ and $M_{\rm B}$ with $1/g^2$ effects, and secondly the comparison is performed in a completely consistent way in terms of $1/d$ expansion. In particular, the baryon hopping effects in the spatial direction ($\mathscr{O}(1/\sqrt{d})$ effects) is precisely evaluated.

The organization of this proceedings is as follows. In Sec. 2, we evaluate the next to leading order contribution of the strong coupling expansion, and derive the analytic expression of the effective potential. From the minimum search at finite couplings, we investigate the phase diagram evolution. In Sec. 3, we investigate the analytic relation between $N_c\mu_c$ and $M_{\rm B}$ and their evolution at finite couplings by applying the formulation obtained in Sec. 2 in a zero temperature treatment. Finally we provide the concluding remarks in Sec. 4.

2. Phase diagram evolution

In this section, we obtain the analytic expression of the effective potential, and investigate the phase diagram evolution with the finite coupling effects.

2.1 Formulation

We start from the lattice QCD action and the partition function with one species of staggered fermion (χ),

$$Z = \int \mathscr{D}[\chi,\bar{\chi},U_0,U_j]\; e^{-S_F^{(\tau)}-S_F^{(s)}-S_G-m_0\sum_x(\bar{\chi}\chi)_x} \tag{2.1}$$

$$S_F^{(\tau)} = \frac{1}{2}\sum_x\left[e^{\mu}\bar{\chi}_x U_{0,x}\chi_{x+\hat{0}} - e^{-\mu}(h.c)\right] \tag{2.2}$$

$$S_F^{(s)} = \frac{1}{2}\sum_x\sum_{j=1}^{d}\eta_{j,x}\left[\bar{\chi}_x U_{j,x}\chi_{x+\hat{j}} - (h.c)\right] \tag{2.3}$$

$$S_G = \frac{2N_c}{g^2}\sum_x\sum_{\nu,\rho}\left[1-\frac{1}{2N_c}\mathrm{tr}_c\left(U_{\nu\rho,x}+U^{\dagger}_{\nu\rho,x}\right)\right], \tag{2.4}$$

where U_0 and U_j represent the temporal and spatial link variables respectively, and $\eta_{j,x}$ denotes the staggered phase factor $(-1)^{x_0+\cdots+x_{j-1}}$. In the following, we consider the color SU($N_c=3$) case in $3+1$ dimension ($d=3$). We introduce the lattice chemical potential μ following the work in

Ref. [22]. We take account of the finite temperature (T) effect by imposing the periodic and anti-periodic boundary conditions on gluon and quarks respectively. Then it is known that the specified gauge (called Polyakov gauge) [6],

$$U_0(\tau,\mathbf{x}) = \mathrm{diag}\{e^{iT\theta^1(\mathbf{x})},\cdots,e^{iT\theta^{N_c}(\mathbf{x})}\}\ , \tag{2.5}$$

can be taken with respect to the periodicity. Here $\mathbf{1}_c$ represents the $N_c\times N_c$ color unit matrix.

In the strong coupling region ($g\gg 1$), plaquette contributions ($\propto 1/g^2$) can be approximated by utilizing the expansion in terms of $1/g^2$ (Strong Coupling Expansion). With the nilpotent nature of the quark fields $(\chi,\bar{\chi})$, the integral over the links can be exactly evaluated, and leads to a sum over the local color singlets *i.e.* mesonic and baryonic composites. In the current formulation, we first integrate out the only spatial link (U_j) variables while the temporal link (U_0) is kept and evaluated later with respect to the finite temperature effect. We consider the leading ($S_{\rm SCL}$) and the next-to-leading order ($\Delta S_\beta^{(\tau,s)}$) terms in the strong coupling ($1/g^2$) expansion, and the leading order in the $1/d$ expansion [23]. Then the effective action is found to be,

$$S = S_{\rm SCL} + \Delta S_\beta^{(\tau)} + \Delta S_\beta^{(s)} + \mathscr{O}(1/\sqrt{d}, 1/g^4) \tag{2.6}$$

$$S_{\rm SCL} = S_F^{(\tau)} + m_0\sum_x M_x - \frac{1}{2}\sum_{xy} M_x V_{xy} M_y \tag{2.7}$$

$$\Delta S_\beta^{(\tau)} = \frac{1}{4N_c^2 g^2}\sum_{x,j>0}(V_x^+ V_{x+\hat{j}}^- + V_x^+ V_{x-\hat{j}}^-) \tag{2.8}$$

$$\Delta S_\beta^{(s)} = -\frac{1}{8N_c^4 g^2}\sum_{x,k>j>0} M_x M_{x+\hat{j}} M_{x+\hat{k}} M_{x+\hat{k}+\hat{j}}\ , \tag{2.9}$$

where $M_x = \bar{\chi}_x^a\chi_x^a$, $V^+ = e^{\mu}\bar{\chi}U_0\chi$, $V^- = e^{-\mu}\bar{\chi}U_0^\dagger\chi$, and the matrix $V_{xy} = \sum_j(\delta_{x+\hat{j},y}+\delta_{x-\hat{j},y})/2N_c$ represents the meson hopping. Due to the existence of the temporal link U_0, the non-local color singlets V^+, V^- appear, which play an important role in the phase diagram evolution.

Now some kinds of interactions (MVM and $\Delta S_F^{(s,\tau)}$) appear as a consequence of U_j integral. To evaluate them, we apply the new method named *Extended Hubbard-Stratonovich Transformation* [17], where two auxiliary fields (φ,ϕ) are introduced to the original composite fields (A,B),

$$\begin{aligned} e^{\alpha AB} &= \int d\varphi\, d\phi\, e^{-\alpha\{\varphi^2-(A+B)\varphi+\phi^2-i(A-B)\phi\}} \\ &\approx e^{-\alpha\{\varphi^2-(A+B)\varphi-\phi^2+(A-B)\phi\}}\ . \end{aligned} \tag{2.10}$$

Here α is an arbitrary real constant. In the second line, we have applied the mean field and the saddle point approximation for φ and ϕ, respectively, provided that the stationary value of ϕ is pure imaginary. For the temporal plaquette action $\Delta S_\beta^{(\tau)}$, we substitute $(\alpha,A,B) = (1/4N_c^2g^2, -V_x^+, V_{x+\hat{j}}^-)$, and obtain,

$$\Delta S_\beta^{(\tau)} \approx \frac{1}{4N_c^2g^2}\sum_{x,j>0}\Big[\varphi_\tau^2 + (V_x^+ - V_{x+\hat{j}}^-)\varphi_\tau\ -\phi_\tau^2 - (V_x^+ + V_{x+\hat{j}}^-)\phi_\tau\Big] + (j\leftrightarrow -j)\ . \tag{2.11}$$

For the spatial plaquette action $\Delta S_\beta^{(s)}$ in Eq. (2.9), we obtain the effective action in a similar way, except that the saddle point field ϕ_s is found to give no effects. Effective action terms from $\Delta S_\beta^{(\tau,s)}$

have similar forms to those in the effective action in the strong coupling limit (SCL, $S_{\rm SCL}$). Here we assume the auxiliary fields $\varphi_{\tau,s}$ and ϕ_τ are constant. Considering up to $\mathscr{O}(1/g^4)$, the $S_{\rm SCL}$ and $\Delta S_\beta^{(\tau,s)}$ are combined to be,

$$\begin{aligned} S_{\rm eff} =& \frac{1}{2}(1+\beta_\tau\varphi_\tau)\sum_x\left(e^{-\beta_\tau\phi_\tau}V_x^+ - e^{\beta_\tau\phi_\tau}V_x^-\right) \\ & - \frac{C_M}{2}\sum_{xy}M_xV_{xy}M_y + m_0\sum_x M_x + N_\tau L^d\left[\frac{\beta_\tau}{2}(\varphi_\tau^2-\phi_\tau)^2 + \frac{d\beta_s}{2}\varphi_s^2\right] , \end{aligned} \tag{2.12}$$

where $\beta_\tau = d/N_c^2g^2$, $\beta_s=(d-1)/8N_c^4g^2$, $C_M = 1+N_c\beta_s\varphi_s$, and L and N_τ are the lattice sizes in spatial and temporal directions. By expanding $e^{\pm\beta_\tau\phi_\tau}$ up to $\mathscr{O}(1/g^4)$, it is easily confirmed that the first line in Eq. (2.12) reproduces the coupling part of (V^+,V^-) and (φ_τ,ϕ_τ) in Eq. (2.11). In the same procedure to that in SCL [23], we introduce the auxiliary field σ for the quadratic term of the mesonic composite M in Eq. (2.12),

$$\begin{aligned} \exp\Big[\frac{C_M}{2}\sum_{xy}M_xV_{xy}M_y\Big] &= \int\mathscr{D}\sigma\ \exp\Big[C_M\Big[-\frac{1}{2}\sum_{j,xy}\sigma_xV_{xy}\sigma_y - \sum_x\sigma_xV_{xy}M_y\Big]\Big] \\ &\simeq \exp\Big[C_M\frac{d}{N_c}\Big[-\frac{N_\tau L^d}{2}\sigma^2 - \sigma\sum_y M_y\Big]\Big] . \end{aligned} \tag{2.13}$$

In the second line, we assumed that the auxiliary field σ took a constant equilibrium value, and then the factor (d/N_c) comes from the meson hopping matrix V_{xy}. Here it is known that the σ in this prescription corresponds to the constant scalar meson $\langle\bar\psi\mathbf{1}_{\rm spin}\otimes\mathbf{1}_{\rm taste}\psi\rangle$ in the Dirac fermion (ψ) picture [24, 25].

Now the effective action is reduced to the bilinear form in terms of the quark fields $(\chi,\bar\chi)$,

$$S_{\rm eff} = (1+\beta_\tau\varphi_\tau)\sum_{xy}\bar\chi_xG^{-1}_{xy}\chi_y + N_\tau L^d\Big[\frac{d}{4N_c}\sigma^2 + d\beta_s\varphi_s\sigma^2 + \frac{d\beta_s}{2}\varphi_s^2 + \frac{\beta_\tau}{2}\big(\varphi_\tau^2-\phi_\tau^2\big)\Big] \tag{2.14}$$

$$G^{-1}_{xy} = \frac{1}{2}\Big(e^{\tilde\mu}U_{0,x}\delta_{x+\hat0,y} - e^{-\tilde\mu}U^\dagger_{0,x}\delta_{x-\hat0,y}\Big)\delta_{\mathbf{xy}} + m_{\rm q}\delta_{xy} \tag{2.15}$$

$$\tilde\mu = \mu - \beta_\tau\phi_\tau\ , \qquad m_{\rm q} = \frac{m_0+(d/2N_c)\sigma(1+2N_c\beta_s\varphi_s)}{1+\beta_\tau\varphi_\tau}\ . \tag{2.16}$$

The finite coupling $1/g^2$ effects are included in some terms with a factor $\beta_{\tau,s}$. It is interesting that quark chemical potential and the constituent quark mass are modified due to the finite coupling effects $(\varphi_{\tau,s},\phi_\tau)$. In particular, the temporal plaquette effects φ_τ,ϕ_τ cause the suppression of quark chemical potential and the constituent quark mass. As shown in the next subsection, this mechanism is essential to the phase diagram evolution. In Eq. (2.14) and (2.15), the quark kinetic term has the same functional form as the strong coupling limit case except for some modification due to $\varphi_{\tau,s}$ and ϕ_τ. Hence the quark and temporal link integral can be evaluated in the same manner as the strong coupling limit. The resultant effective potential (free energy density) is a function of the

auxiliary fields $\Phi=(\sigma,\varphi_{\tau,s},\phi_\tau)$, the temperature T and the effective quark chemical potential $\tilde{\mu}$,

$$\mathscr{F}_{\rm eff}(\Phi;T,\tilde{\mu}) = \mathscr{F}_{\rm Aux}(\Phi)+\mathscr{V}_{\rm q}(m_{\rm q}(\Phi);T,\tilde{\mu}) \tag{2.17}$$

$$\mathscr{F}_{\rm Aux}(\Phi) = \frac{d}{4N_c}\sigma^2+d\beta_s\varphi_s\sigma^2+\frac{d\beta_s}{2}\varphi_s^2+\frac{\beta_\tau}{2}\left(\varphi_\tau^2-\phi_\tau^2\right)-N_c\log\left(1+\beta_\tau\varphi_\tau\right) \tag{2.18}$$

$$\mathscr{V}_{\rm q}(m_{\rm q}(\Phi);T,\tilde{\mu}) = -T\log\left[X_{N_c}+2\cosh\left[\frac{N_c\tilde{\mu}}{T}\right]\right] \tag{2.19}$$

$$X_{N_c} = \frac{\sinh\left[(N_c+1)E(m_{\rm q}(\Phi))/T\right]}{\sinh\left[E(m_{\rm q}(\Phi))/T\right]}\ , \tag{2.20}$$

where $E(m_{\rm q}(\Phi))=\sinh^{-1}\left[m_{\rm q}(\Phi)\right]$ corresponds to the quark excitation energy. Now we have introduced four kinds of auxiliary fields $\Phi=(\sigma,\varphi_s,\varphi_\tau,\phi_\tau)$, and it seems to contain some redundant degrees of freedom. This can be cared by considering the constraints $\partial\mathscr{F}_{\rm eff}(\Phi)/\partial\Phi=0$. From $\partial\mathscr{F}_{\rm eff}(\Phi)/\partial\sigma=0$, we obtain $\sigma=-\partial_{m_q}\mathscr{V}_{\rm q}+\mathscr{O}(1/g^2)$, and the constraints for $\varphi_{\tau,s}$ are also derived by utilizing this relation,

$$\varphi_s = 2\sigma^2 \tag{2.21}$$

$$\varphi_\tau = \sigma\Big(\frac{d}{2N_c}\sigma+m_0\Big)-N_c+\mathscr{O}(1/g^2)\ . \tag{2.22}$$

By substituting equilibrium values of $\varphi_{\tau,s}$, the effective potential is obtained as functions of (σ,ϕ_τ) and $(T,\tilde{\mu})$,

$$\mathscr{F}_{\rm eff} = \mathscr{F}_{\rm Aux}(\sigma,\phi_\tau)+\mathscr{V}_{\rm q}(m_{\rm q}(\sigma),\tilde{\mu}(\phi_\tau),T)\ , \tag{2.23}$$

$$\mathscr{F}_{\rm Aux} = \frac{1}{2}b_\sigma\sigma^2+\frac{\beta_\tau}{2}\sigma^2(m_{\rm q}^{\rm SCL})^2+\frac{3d\beta_s}{2}\sigma^4-\frac{\beta_\tau}{2}\phi_\tau^2\ , \tag{2.24}$$

$$m_{\rm q} = m_q^{\rm SCL}(1-N_c\beta_\tau)+\beta_\tau\sigma(m_q^{\rm SCL})^2+2d\beta_s\sigma^3\ , \tag{2.25}$$

where $b_\sigma=d/2N_c$, $m_{\rm q}^{\rm SCL}=b_\sigma\sigma+m_0$, and we have omitted higher order terms of $\mathscr{O}(1/g^4)$ in $\mathscr{F}_{\rm Aux}$ and $m_{\rm q}$. The chiral condensate σ is regarded as a dynamical parameter, and the phase diagram is investigated by performing the minimum search of the effective potential $\mathscr{F}_{\rm eff}$ with a remnant constraint $\partial\mathscr{F}_{\rm eff}(\Phi)/\partial\phi_\tau=0$, which leads,

$$\phi_\tau=-\frac{\partial\mathscr{F}_{\rm eff}}{\partial\mu}=\frac{2N_c\sinh(N_c\tilde{\mu}/T)}{X_{N_c}+2\cosh(N_c\tilde{\mu}/T)}\equiv\rho_q\ . \tag{2.26}$$

2.2 Results and Discussion

Considering the expansion $\mathscr{F}_{\rm eff}=\sum_n C_n\sigma^n$, the critical line for the second order transition is given by,

$$C_2=\frac{1}{2}b_\sigma-\frac{b_\sigma^2N_c(N_c+1)(N_c+2)(1-N_c\beta_\tau)^2}{6T(N_c+1+2\cosh(N_c\tilde{\mu}/T))}=0\ . \tag{2.27}$$

In some region, the Wigner phase ($\sigma=0$) is not the global $\mathscr{F}_{\rm eff}$ minimum on the phase transition line given by Eq. (2.27), then the phase transition is the first order. First we concentrate on the critical temperature along the T axis ($\mu=0$). By solving $C_2|_{\mu=0}=0$, we find the second order

phase transition temperature $T_c^{(\rm 2nd)}|_{\mu=0}$ is expressed by using that in the strong coupling limit $T_c^{(\rm SCL,2nd)}|_{\mu=0}$ with a suppression factor due to the finite coupling effects,

$$T_c^{(\rm 2nd)}|_{\mu=0} = T_c^{(\rm SCL,2nd)}|_{\mu=0}\,(1-N_c\beta_\tau)^2\,, \qquad T_c^{(\rm SCL,2nd)}|_{\mu=0} = \frac{d(N_c+1)(N_c+2)}{6(N_c+3)}\,. \tag{2.28}$$

The decrease of the critical temperature is mainly caused by the suppression factor $(1+\beta_\tau\varphi_\tau)$ in the constituent quark mass expressed in Eq. (2.16). As shown in the left panel of Fig. 1, the high T transition becomes the first order in the region $6/g^2 > 1.40$ while it is the second order around SCL [10, 11]. This change is caused by the higher order terms of σ in $\mathscr{F}_{\rm Aux}$ and $m_{\rm q}$. The calculated critical temperature is in agreement with the Monte-Carlo (MC) results with $N_\tau = 2$ at strong coupling [26]. Compared to the quenched ($m_0 = \infty$) result $\beta_c = 6/g_c^2 = 5.097(1)$ [27] at $N_\tau = 2$, the critical inverse coupling decreases with small quark masses; $\beta_c = 3.81(2)(m_0 = 0.05)$ and $\beta_c = 3.67(2)(m_0 = 0.025)$ [26] on a $8^3\times 2$ lattice with one species of staggered fermions ($N_f = 4$). These MC results with small quark masses are consistent with the present result $\beta_c = 3.61$ at $T_c = 1/N_\tau = 1/2$ in the chiral limit, as shown in the right panel of Fig. 1. The suppression of T_c would be a natural consequence of finite coupling, since hadrons are less bound than in SCL.

We numerically find that the chiral phase transition along the μ axis is the first order, and the critical chemical potential with finite coupling ($\mu_c^{(\rm 1st)}$) is not largely modified from the strong coupling limit value $\mu_c^{(\rm SCL,1st)}$ (*c.f.* $\mu_c^{(\rm 1st)} \simeq 0.59$ at $6/g^2 = 3.0$ and $\mu_c^{(\rm SCL,1st)} \simeq 0.55$). This small modification is understood as follows: In the low temperature region, the first order phase transition is described in terms of the competition between the quark chemical potential and the constituent quark mass. Since the temporal plaquette leads to the suppression of both, the relative relations between them are not largely changed. Hence $\mu_c^{(\rm 1st)} \simeq \mu_c^{(\rm SCL,1st)}$ follows.

Thus we find the significant difference in the suppressions of the critical values $T_c^{(\rm 1st\ or\ 2nd)}$ and $\mu_c^{(\rm 1st)}$. As a result, the ratio $R = \mu_c^{(\rm 1st)}/T_c^{(\rm 1st\ or\ 2nd)}$ increases and become closer to the empirical value $R \gg 1$, as the coupling decreases. In Fig. 2, we show the phase diagram with $6/g^2 = 3.0$ and $N_c = 3$ in the chiral limit as a typical example. We find the ratio $R \simeq 1.0$, which is much larger than the strong coupling limit value $R_{\rm SCL} \sim 0.3 - 0.45$.

3. Baryon Mass Puzzle

As explained in the introduction, the strong coupling limit encounters the Baryon Mass Puzzle (BMP); the chiral phase transition occurs before the baryon chemical potential $N_c\mu$ exceeds the baryon mass $M_{\rm B}$. In the previous section, we learned that the effective chemical potential is modified to $\tilde{\mu} = \mu - \beta_\tau\phi_\tau$ due to the finite coupling effect. Naïvely, the result in the strong coupling limit $N_c\mu_c < M_{\rm B}$ may be replaced with $N_c\tilde{\mu}_c = N_c(\mu_c - \beta_\tau\phi_\tau) < M_{\rm B}$. Then it could be possible that the plausible relation $N_c\mu_c \geq M_{\rm B}$ is realized due to the finite coupling effect ($\beta_\tau\phi_\tau$). In this section, we explicitly investigate this mechanism.

3.1 Formulation

The analytic expression of the baryon mass is obtained from the mass pole of the baryon propagator. Therefore it is necessary to consider the baryon hopping effects, which are included in the next to leading order (NLO, $\mathscr{O}(1/\sqrt{d})$) of the $1/d$ expansion [23]. We investigate the $\mathscr{O}(1/\sqrt{d})$

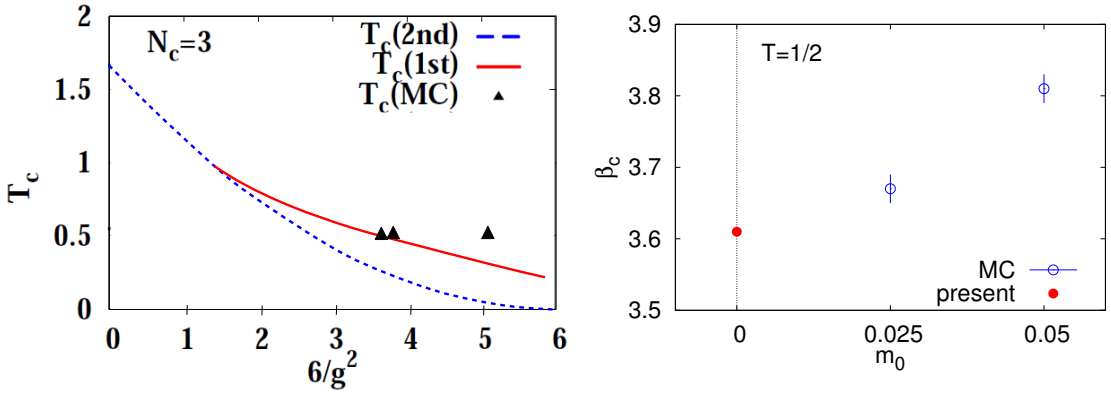

Figure 1: Left: The coupling dependence of critical temperature. The red solid and blue dashed lines represent the first and second order transition, respectively. The MC results are also plotted (small triangles): From the left $m_0 = 0.025,\ 0.05$ [26] and $m_0 = \infty$ [27]. Right: Comparison of the critical coupling $\beta_c = 6/g_c^2$ at $N_\tau = 2$ ($T = 1/2$) in MC simulations (open circles) and the present result (filled circle). MC results are taken from Ref. [26].

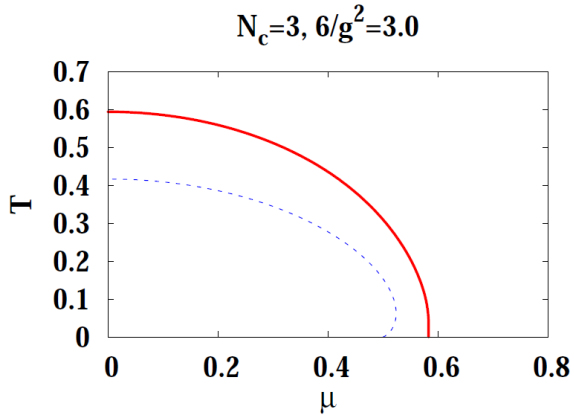

Figure 2: The phase diagram at $\beta = 6/g^2 = 3.0$ The red solid and blue dashed lines represent the first and second order transition, respectively. The actual transition is described by the red solid line.

effects in the strong coupling limit, while we restrict our analysis to the leading order of $1/d$ expansion in the NLO of the strong coupling expansion. In order to investigate the BMP, it is enough to consider the zero temperature treatment. Those set-ups may be the simplest to study the finite coupling effects to BMP. The effective action can be obtained by adding the $\mathcal{O}(1/\sqrt{d})$ effects of the strong coupling limit,

$$S_{\rm eff}^{(b)} = \frac{(-1)^{N_c(N_c-1)/2}}{2^{N_c}} \sum_{j=1}^{d} \eta_{j,x} \left[\bar{B}_x B_{x+\hat{j}} + (-1)^{N_c} (h.c.) \right] , \tag{3.1}$$

to Eq. (2.12). In the zero temperature treatment, the temporal link (U_0) is simply integrated in the same way as the spatial links U_j, hence the Polyakov gauge Eq. (2.5) is not used here. However we

would like to emphasize that U_0 is integrated after introducing the auxiliary fields φ_τ, ϕ_τ in order to include the modification $\mu \to \tilde{\mu}$.

The integral over U_0 leads to the effective action,

$$S_{\rm eff} = -\frac{1}{2}M\cdot V_M\cdot M - \bar{B}\cdot V_B\cdot B + m_0\sum_x M_x + N_\tau L^d\left[\frac{\beta_\tau}{2}(\varphi_\tau^2-\phi_\tau)^2+\frac{d\beta_s}{2}\varphi_s^2\right], \quad (3.2)$$

$$V_M(xy) = \frac{\left(1+\beta_\tau\varphi_\tau\right)^2}{4N_c}\left[\delta_{x+\hat{0},y}+\delta_{x-\hat{0},y}\right]+\left(\frac{1}{4N_c}+\beta_s\varphi_s\right)\sum_j\left[\delta_{x+\hat{j},y}+\delta_{x-\hat{j},y}\right] \quad (3.3)$$

$$V_B(xy) = (-1)^{N_c(N_c-1)/2}\left[\left[\frac{1+\beta_\tau\varphi_\tau}{2}\right]^{N_c}\left[e^{N_c\tilde{\mu}}\delta_{x+\hat{0},y}+(-1)^{N_c}e^{-N_c\tilde{\mu}}\delta_{x-\hat{0},y}\right]\right.$$
$$\left.+\eta_{j,x}\left[\delta_{x+\hat{j},y}+(-1)^{N_c}\delta_{x-\hat{j},y}\right]\right], \quad (3.4)$$

where " $\cdot$ " represents the summation over the spacetime index (x,y). The mesonic composite term MV_MM in the effective action $S_{\rm eff}$ is evaluated in the same way as Eq. (2.13), and the baryon fields $b,\bar{b}$ are also introduced via the similar method [7],

$$\exp\left[\bar{B}\cdot V_B\cdot B\right] = \mathrm{Det}\,V_B\int\mathscr{D}[b,\bar{b}]\exp\left[-\bar{b}\cdot V_B^{-1}\cdot b+\bar{B}\cdot b+\bar{b}\cdot B\right]. \quad (3.5)$$

In the zero temperature treatment, there is no hopping of the staggered quark $(\chi,\bar{\chi})$ after the link integral, and we can perform the path integral over $(\chi,\bar{\chi})$ by expanding the exponential at each lattice site. This simply causes the constant shift to the baryon propagator V_B^{-1}, which is evaluated by utilizing the Fourier transformation. These are the parallel works to the strong coupling limit case [7], and the resultant effective potential becomes,

$$\mathscr{F}_{\rm eff} = \frac{C_\sigma}{2}\sigma^2+\frac{\beta_\tau}{2}(\varphi_\tau^2-\phi_\tau^2)+\frac{d\beta_s}{2}\varphi_s^2-N_c\log\left[1+\beta_\tau\varphi_\tau\right]+\mathscr{V}_{\rm B}, \quad (3.6)$$

$$\mathscr{V}_{\rm B} = -\frac{1}{N_\tau L^d}\sum_{\mathbf{p}}\begin{cases}\tilde{\mu}N_c & E_{\rm B}(\mathbf{p})\le\tilde{\mu}N_c\\ E_{\rm B}(\mathbf{p}) & E_{\rm B}(\mathbf{p})\ge\tilde{\mu}N_c\end{cases}, \quad (3.7)$$

where $E_{\rm B}(\mathbf{p})$ corresponds to the baryon excitation energy,

$$E_{\rm B}(\mathbf{p}) = \sinh^{-1}\left[\frac{1}{(1+\beta_\tau\varphi_\tau)^{N_c}}\sqrt{\sum_j\sin^2 p_j+\frac{1}{4}\left(2(m_0+C_\sigma\sigma)\right)^{2N_c}}\right] \quad (3.8)$$

$$C_\sigma = \frac{d+1}{2N_c}+\frac{\beta_\tau}{N_c}\varphi_\tau+2d\beta_s\varphi_s+\mathscr{O}(1/g^4). \quad (3.9)$$

Here we concentrate on the zero momentum mode $\mathbf{p}\to\mathbf{0}$, where we obtain the baryon mass $M_{\rm B}$ as,

$$E_{\rm B}(\mathbf{p},\sigma,\varphi_{s,\tau},\phi_\tau)\to M_{\rm B}(\sigma,\varphi_{s,\tau},\phi_\tau) = \sinh^{-1}\left[\frac{1}{2}\left(\frac{2(m_0+C_\sigma\sigma))}{1+\beta_\tau\varphi_\tau}\right)^{N_c}\right]. \quad (3.10)$$

We can numerically confirm that replacing $E_{\rm B}$ with $M_{\rm B}$ leads to at most a few percent error. It is interesting that the finite φ_τ causes stronger suppression of the baryon mass rather than the constituent quark mass, and this is the different point from the previous section.

As in the phase diagram investigation, the redundant degrees of freedom are reduced by utilizing the stationary constraints for the auxiliary fields,

$$\sigma = -\frac{\partial \mathscr{V}_{\rm B}}{\partial m_q'}\,, \qquad \varphi_s = 2\sigma^2\,, \qquad \varphi_\tau = N_c + \frac{\sigma^2}{N_c} + \mathscr{O}(1/g^2)\,. \tag{3.11}$$

Substituting the second and third expressions for φ_s and φ_τ in Eq. (3.7), we obtain the final expression of the effective potential,

$$\mathscr{F}_{\rm eff} = \sum_l \frac{C_l}{l}\sigma^l - \frac{\beta_\tau}{2}\phi_\tau^2 - \begin{cases} \tilde{\mu}N_c & M_{\rm B}(\sigma) \le \tilde{\mu}N_c \\ M_{\rm B}(\sigma) & M_{\rm B}(\sigma) \ge \tilde{\mu}N_c \end{cases} \tag{3.12}$$

$$\Big(C_2,\, C_4\Big) = \Big(\frac{d+1}{2N_c} + \beta_\tau, \quad \frac{4\beta_\tau}{N_c^2} + 16\, d\beta_s\Big)\,. \tag{3.13}$$

Now the baryon mass $M_{\rm B}$ becomes the function of the chiral condensate σ, and its expression is obtained by substituting the second and third expressions in (3.11) for C_σ in (3.10). We analyze the obtained effective action Eq. (3.12) with the stationary constraints for ϕ_τ, which leads,

$$\phi_\tau = \begin{cases} N_c & (M_{\rm B} \le N_c(\mu - \beta_\tau N_c)) \\ (1/\beta_\tau)(\mu - M_{\rm B}/N_c) & (N_c(\mu-\beta_\tau N_c) \le M_{\rm B} \le N_c\mu) \\ 0 & (N_c\mu \le M_{\rm B}) \end{cases}\,. \tag{3.14}$$

3.2 Results and Discussion

In the left panel of Fig. 3, we show the effective potential as a function of the chiral condensate σ for several values of quark chemical potential μ. We find the two local minimum structure of the effective potential, and the chiral phase transition is described by those competitions. Hence the critical value of the chiral condensates σ_c and the critical quark chemical potential μ_c satisfy $\mathscr{F}_{\rm eff}(\sigma = 0) = \mathscr{F}_{\rm eff}(\sigma = \sigma_c)$, or equivalently,

$$-N_c\mu_c + \frac{\beta_\tau}{2}N_c^2 = -M_{\rm B}(\sigma_c) + \sum_l \frac{C_l}{l}\sigma_c^l\,, \tag{3.15}$$

where we used Eq. (3.14). The left and right hand sides in Eq. (3.15) correspond to the left and right minima in the red line in the figure, respectively. This equation gives us the explicit relation between the critical baryon chemical potential $N_c\mu_c$ and the baryon mass $M_{\rm B}(\sigma_c)$ in the vacuum.

Now let us move on the investigation of the Baryon Mass Puzzle (BMP). First we consider the strong coupling limit case. Then the second term in the left hand side of Eq. (3.15) disappears, and we find that there exists the discrepancy between $N_c\mu_c$ and $M_{\rm B}$ due to the chiral condensate contributions $\sum_l (C_l/l)\sigma_c^l$. As a result, the relation $N_c\mu_c < M_{\rm B}$ or $N_c\mu_c/M_{\rm B} \simeq 0.52 < 1.0$ follows. This is the origin of the BMP. The similar discussion at strong coupling limit can be found in Ref. [16].

Next we consider the finite coupling case. Then second term in the left hand side of Eq. (3.15) increases as the coupling decreases, and has an effect to cancel the chiral condensate $\sum_l (C_l/l)\sigma_c^l$ in the right hand side. Therefore the ratio $N_c\mu_c/M_{\rm B}$ becomes larger. This is illustrated in the right panel of Fig. 3. Thus the finite coupling effects make the BMP softer, however we find that this is not enough to solve the BMP: The ratio $N_c\mu_c/M_{\rm B}$ is still less than 1.0 for the relatively large value of $\beta = 6/g^2$.

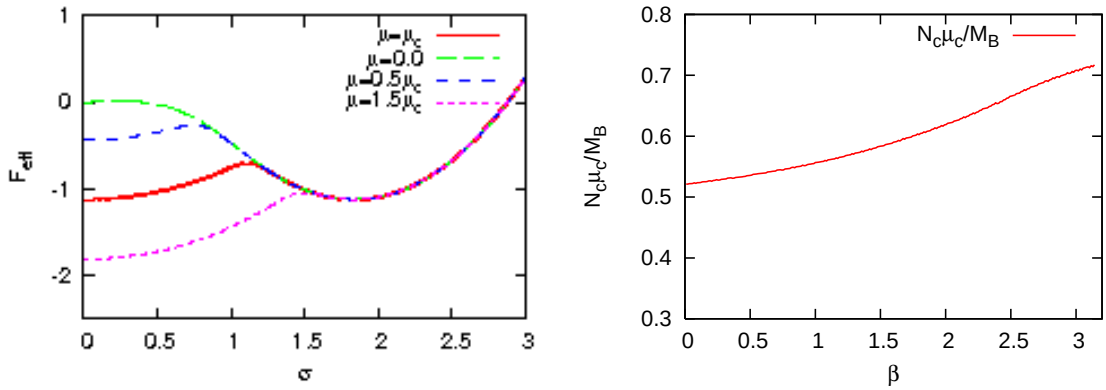

Figure 3: Left: The effective potential as a function of the chiral condensate at some chemical potential values. The red solid line corresponds to the effective potential at the critical chemical potential. Right: The ratio $N_c\mu_c/M_{\rm B}$ as a function of the inverse coupling squared $\beta = 6/g^2$.

4. Concluding Remarks

We have investigated the phase diagram and the baryon mass ($M_{\rm B}$) in the strong coupling lattice QCD with one species of staggered fermions at finite quark chemical potential (μ) and/or finite temperature (T). In particular, their evolution with the finite coupling $(1/g^2)$ was studied. In the mean field approximation, we formulated the treatment of temporal plaquette effects by introducing some new auxiliary fields which give rise to the suppression of (μ) and the constituent quark mass (m_q). Then the ratio (μ_c/T_c) was found to become larger and closer to the empirical value, as the coupling decreases. And the second order transition along the temperature axis evolves to the first order, and the critical value T_c is found to be consistent with lattice Monte-Carlo simulation results. The same suppression mechanism of μ was found to make the ratio $N_c\mu_c/M_{\rm B}$ larger, however that is not enough to form nuclear matter.

Acknowledgments

We would like to thank Philippe de Forcrand and Michael Fromm for useful discussions. We thank Barak Bringoltz for stimulating discussions. This work is supported in part by KAKENHI, 17070002 (Priority area), and by the Ministry of Education, Science, Sports and Culture, Grant-in-Aid for Scientific Research under the grant numbers, 19540252, and the Yukawa International Program for Quark-hadron Sciences (YIPQS).

References

[1] For a recent review, see B. Muller and J. L. Nagle, *Results from the Relativistic Heavy Ion Collider, Ann. Rev. Nucl. Part. Sci.* **56** (2006) 93 [arXiv:nucl-th/0602029].

[2] For a review, see K. Rajagopal and F. Wilczek, *The condensed matter physics of QCD,* [arXiv:hep-ph/0011333].

[3] L. McLerran and R. D. Pisarski, *Phases of Cold, Dense Quarks at Large N_c, Nucl. Phys.* A **796** (2007) 83 [arXiv:0706.2191 [hep-ph]]; Y. Hidaka, L. D. McLerran and R. D. Pisarski, *Baryons and*

the phase diagram for a large number of colors and flavors, Nucl. Phys. A **808** (2008) 117 [arXiv:0803.0279 [hep-ph]].

[4] For a recent review, see O. Philipsen, *The QCD phase diagram at zero and small baryon density, PoS* **LAT2005** (2006) 016 [PoS **JHW2005** (2006) 012] [arXiv:hep-lat/0510077].

[5] N. Kawamoto and J. Smit, *Effective Lagrangian And Dynamical Symmetry Breaking in Strongly Coupled Lattice QCD,* Nucl. Phys. B **192** (1981) 100.

[6] P. H. Damgaard, N. Kawamoto and K. Shigemoto, *Strong Coupling Analysis Of The Chiral Phase Transition At Finite Temperature, Nucl. Phys.* **B264**, (1986) 1 .

[7] P. H. Damgaard, D. Hochberg and N. Kawamoto, *Effective Lagrangian Analysis Of The Chiral Phase Transition at Finite Density, Phys. Lett.* **B158**, (1985) 239.

[8] H. Kluberg-Stern, A. Morel, O. Napoly and B. Petersson, *Spontaneous Chiral Symmetry Breaking For A U(N) Gauge Theory On A Lattice, Nucl. Phys.* B **190** (1981) 504.

[9] Y. Nishida, K. Fukushima and T. Hatsuda, *Thermodynamics of strong coupling 2-color QCD with chiral and diquark condensates, Phys. Rept.* **398** (2004) 281 [arXiv:hep-ph/0306066].

[10] K. Fukushima, *Toward understanding the lattice QCD results from the strong coupling analysis, Prog. Theor. Phys. Suppl.* **153** (2004) 204 [arXiv:hep-ph/0312057]; Y. Nishida, *Phase structures of strong coupling lattice QCD with finite baryon and isospin density, Phys. Rev.* D **69** (2004) 094501 [arXiv:hep-ph/0312371].

[11] N. Kawamoto, K. Miura, A. Ohnishi and T. Ohnuma, *Phase diagram at finite temperature and quark density in the strong coupling limit of lattice QCD for color SU(3), Phys. Rev.* D **75** (2007) 014502 [arXiv:hep-lat/0512023].

[12] P. de Forcrand and S. Kim, *The spectrum of lattice QCD with staggered fermions at strong coupling, Phys. Lett.* B **645** (2007) 339 [arXiv:hep-lat/0608012].

[13] I. M. Barbour, S. E. Morrison, E. G. Klepfish, J. B. Kogut and M. P. Lombardo, *The critical points of strongly coupled lattice QCD at nonzero chemical potential, Phys. Rev.* D **56** (1997) 7063 [arXiv:hep-lat/9705038].

[14] N. Bilic, K. Demeterfi and B. Petersson, *Strong coupling analysis of the chiral phase transition at finite chemical potential and finite temperature, Nucl. Phys.* B **377** (1992) 651.

[15] T. Jolicoeur, H. Kluberg-Stern, M. Lev, A. Morel and B. Petersson, *The Strong Coupling Expansion Of Lattice Gauge Theories With Susskind Fermions, Nucl. Phys.* B **235** (1984) 455.

[16] B. Bringoltz, *Chiral crystals in strong-coupling lattice QCD at nonzero chemical potential, JHEP* **0703** (2007) 016 [arXiv:hep-lat/0612010].

[17] K. Miura and A. Ohnishi, *Quarkyonic phase in lattice QCD at strong coupling,* [arXiv:0806.3357 [nucl-th]].

[18] A. Ohnishi, N. Kawamoto and K. Miura, *Brown-Rho Scaling in the Strong Coupling Lattice QCD,* [arXiv:0803.0255 [nucl-th]].

[19] N. Kawamoto, K. Miura and A. Ohnishi, *Meson mass spectrum at finite temperature and density in the strong coupling limit of lattice QCD for color SU(3), PoS* **LAT2007** (2007) 209 [arXiv:0710.1720 [hep-lat]].

[20] A. Ohnishi, N. Kawamoto, K. Miura, K. Tsubakihara and H. Maekawa, *Strong coupling limit/region of lattice QCD, Prog. Theor. Phys. Suppl.* **168** (2007) 261 [arXiv:0704.2823 [nucl-th]].

[21] A. Ohnishi, N. Kawamoto and K. Miura, *Phase diagram at finite temperature and quark density in the strong coupling region of lattice QCD for color SU(3), J. Phys.* G **34** (2007) S655 [arXiv:hep-lat/0701024].

[22] P. Hasenfratz and F. Karsch, *Chemical Potential On The Lattice Phys. Lett.* B **125** (1983) 308.

[23] H. Kluberg-Stern, A. Morel and B. Petersson, *Spectrum Of Lattice Gauge Theories With Fermions From A 1/D Expansion At Strong Coupling, Nucl. Phys.* B **215** (1983) 527.

[24] H. Kluberg-Stern, A. Morel, O. Napoly and B. Petersson, *Flavors Of Lagrangian Susskind Fermions, Nucl. Phys.* B **220** (1983) 447.

[25] M. F. L. Golterman and J. Smit, *Selfenergy And Flavor Interpretation Of Staggered Fermions, Nucl. Phys.* B **245** (1984) 61.

[26] P. de Forcrand, private communication.

[27] A. D. Kennedy, J. Kuti, S. Meyer and B. J. Pendleton, *Where Is The Continuum In Lattice Quantum Chromodynamics?, Phys. Rev. Lett.* **54**, (1985) 87 .